International Refereed Journal of Engineering and Science (IRJES)
ISSN (Online) 2319-183X, (Print) 2319-1821
Volume 14, Issue 6 (Nov. – Dec. 2025), PP. 92-103

Photocatalytic Degradation of Some Industrial Pollutants Using NiO@WO_3-Chitosan Nanocomposite Synthesized via a Green Route

Sevil AKÇAĞLAR
Department of Mechanical Engineering, Faculty of Engineering, Dokuz Eylül University, İzmir, Turkey,
Corresponding Author: sevil.akcaglar@deu.edu.tr

Abstract: *Industrial processes commonly use azo dyes such as Tropaeolin OOO (TOOO) and Eriochrome Black T (EBT), which are environmentally persistent and toxic. This study presents a green-synthesized NiO@WO_3–chitosan nanocomposite using Azadirachta indica for the effective photocatalytic degradation of these dyes under solar irradiation. Characterization revealed semi-crystalline spherical nanoparticles with strong Ni–O–W, Ni–N, and W–N interactions. Under optimum conditions (pH 7, 20 mg catalyst), complete decolorization of 10 mg/L dye solutions was achieved within 3 hours, with degradation efficiencies of 96% for TOOO and 92% for EBT. The reaction followed pseudo-first-order kinetics, supported by the material's high surface area (75 m^2/g) and low band gap energy (2.1 eV). Scavenger analysis confirmed the involvement of •OH, O_2^-•, and h^+ species in the degradation mechanism. The catalyst maintained its activity over eight reuse cycles, demonstrating its potential as a sustainable and cost-effective solution for industrial wastewater treatment.*

Azo dyes such as Tropaeolin OOO (TOOO) and Eriochrome Black T (EBT), widely used in industrial processes, are environmentally persistent and toxic. This study presents a green-synthesized NiO@WO_3-chitosan nanocomposite using Azadirachta indica for effective photocatalytic degradation of these dyes under sunlight. Characterization revealed semi-crystalline spherical particles with strong Ni–O–W, Ni–N, and W–N interactions. Under optimal conditions (pH 7, 20 mg catalyst), complete decolorization of 10 mg/L dye solutions was achieved within 3 hours, with degradation efficiencies of 96% (TOOO) and 92% (EBT). The reaction followed first-order kinetics, supported by the material's high surface area (75 m^2/g), low band gap (2.1 eV), and strong negative zeta potential (−29.5 mV). Scavenger analysis confirmed the involvement of •OH, O_2^-•, and h^+ species in the degradation mechanism. The catalyst remained active over 8 reuse cycles, demonstrating its potential as a sustainable and cost-effective solution for industrial wastewater treatment.

Keywords*: Photocatalysis, Azo dyes, NiO@WO_3-chitosan nanocomposite Tropaeolin OOO (TOOO), Eriochrome Black T (EBT), Green synthesis, Sunlight degradation, Wastewater treatment*

Date of Submission: 14-11-2025 Date of acceptance: 30-11-2025

I. INTRODUCTION

The widespread use of synthetic organic pollutants—such as pesticides, pharmaceuticals, and particularly azo dyes—has contributed significantly to the deterioration of water quality and the escalation of environmental contamination. Among these, azo dyes are of special concern due to their high production volume and persistent nature. Globally, approximately 7×10^7 tons of dyes are utilized annually in industries such as textiles, food processing, and biomedicine, with azo dyes accounting for nearly 80% of this usage [1,2]. These compounds are characterized by the presence of azo groups (–N=N–), which confer strong color but also chemical stability and resistance to degradation.

Tropaeolin OOO (TOOO) and Eriochrome Black T (EBT) are widely used azo dyes known for their intense coloration and applications in textile dyeing and as pH indicators in analytical chemistry [3,4]. However, their stable molecular structure leads to poor biodegradability and environmental persistence. When discharged into aquatic systems, these dyes can hinder photosynthetic activity by blocking sunlight penetration in the epilimnion layer, ultimately disrupting aquatic ecosystems [5]. Furthermore, studies have highlighted the toxicological risks associated with azo dyes, including mutagenic and carcinogenic effects in humans due to their potential to form aromatic amines upon reduction [6,7].

In response to these concerns, regulatory frameworks such as the European Commission's 19th Amendment have proposed limits on the use and discharge of such dyes. Specifically, a maximum permissible exposure limit of 30 mg/kg body weight and an industrial discharge threshold of 0.01–0.05 ppm have been suggested to mitigate health and ecological risks [3].

Various physical, chemical, and biological methods have been employed to remove azo dyes from wastewater, including coagulation, adsorption, advanced oxidation processes, and microbial degradation. However, these methods often suffer from limitations such as high operational costs, low efficiency, long treatment durations, and the generation of secondary pollutants [8,9]. In contrast, photocatalytic degradation using semiconductor nanomaterials offers a promising alternative due to its efficiency, sustainability, and potential for complete mineralization of pollutants.

In particular, green-synthesized photocatalysts have gained increasing attention for their eco-friendly fabrication and enhanced photocatalytic activity. Plant extracts rich in natural surfactants and reducing agents such as quercetin, β-sitosterol, and polyphenolic flavonoids can facilitate the synthesis of nanostructured metal oxides (e.g., NiO, WO_3, ZnO, TiO_2) with reduced reliance on hazardous chemicals [10–12]. This green route not only improves the safety and sustainability of the synthesis process but also enhances the physicochemical properties of the photocatalysts.

Recent efforts have focused on designing hybrid nanocomposites, particularly bimetallic oxide systems such as NiO@WO_3, to overcome the limitations of single-component photocatalysts. Despite the individual advantages of NiO (a p-type semiconductor with high hole mobility) and WO_3 (an n-type semiconductor with visible-light responsiveness), their performance as standalone materials is often hindered by rapid electron–hole recombination and suboptimal light absorption [13,14]. The integration of these oxides into a composite structure, further stabilized with biopolymers like chitosan, can enhance charge separation, surface area, and stability under solar irradiation.

In this study, we report the green synthesis of a NiO@WO_3-chitosan nanocomposite using *Azadirachta indica* (neem) leaf extract and investigate its photocatalytic performance in degrading TOOO and EBT under natural sunlight. The study focuses on structural characterization, optimization of degradation conditions, and mechanistic understanding of the process, highlighting the material's potential for sustainable industrial wastewater treatment.

Chitosan, a biopolymer derived from the deacetylation of chitin, consists primarily of repeating units of D-glucosamine and N-acetyl-D-glucosamine. Due to its excellent biocompatibility, biodegradability, hydrophilicity, and non-toxic nature, chitosan has emerged as a promising support matrix for the development of functional nanocomposites, particularly those involving metal oxides [15]. Its abundant amino and hydroxyl functional groups not only facilitate metal ion chelation but also promote strong interactions with semiconductor surfaces, enhancing structural stability, dispersion, and photocatalytic efficiency of the resulting materials [16].

In recent years, considerable research has focused on the development of chitosan-supported semiconductor nanocomposites to address the growing challenge of organic dye pollutants in water. Single metal oxide semiconductors such as nickel oxide (NiO) and tungsten trioxide (WO_3) exhibit desirable properties including high thermal and chemical stability, photochromism, and photocatalytic activity. These materials have been applied in areas such as gas sensing, water splitting, and dye degradation [17]. However, their effectiveness as photocatalysts under solar light is limited by their relatively high band gaps—3.6 eV for NiO and 2.6–2.8 eV for WO_3—and the rapid recombination of photogenerated electron–hole (e^-/h^+) pairs [17,19].

To address these limitations, the fabrication of heterojunction nanocomposites comprising both n-type and p-type semiconductors has been proposed. In particular, combining NiO (p-type) with WO_3 (n-type) forms a p–n heterojunction that facilitates efficient charge separation and improves photocatalytic performance under visible light [20]. Incorporating chitosan into such bimetallic systems further enhances photocatalytic activity by improving surface properties, controlling particle size, and preventing agglomeration through steric and hydrophilic-hydrophobic interactions during synthesis [9,10].

Several recent studies have demonstrated the efficacy of metal oxide–chitosan composites in dye removal. For instance, Kazemi et al. synthesized a $CuMn_2O_4$/chitosan nanocomposite via a green hydrothermal method, achieving 99% removal of methylene blue at a 1 ppm concentration under sunlight [15]. Sobhani and colleagues have reported on the use of $CuMn_2O_4$/CuMnO nanocomposites prepared via co-precipitation for the efficient removal of organic pollutants without requiring additional capping agents [21]. Similarly, the $CuMn_2O_4/Mn_2O_3$ system, synthesized using sucrose as a green templating agent through a sol–gel method, achieved 78.12% degradation of Remazol Brilliant Blue R (RBBR) under sunlight within 90 minutes using a 30 mg catalyst dose [22]. Sucrose's role in these systems is comparable to that of chitosan in the current study, both acting as natural, cost-effective stabilizing and reducing agents.

Building upon these developments, the present work focuses on the synthesis of a green, sunlight-active NiO@WO_3-chitosan nanocomposite using *Azadirachta indica* leaf extract. The study aims to evaluate its photocatalytic performance in degrading hazardous azo dyes—Tropaeolin OOO (TOOO) and Eriochrome Black T (EBT)—under various experimental conditions. The synergistic effect of the bimetallic oxide system and the biopolymeric matrix is expected to enhance the overall photodegradation efficiency, charge separation, and material stability, offering a sustainable solution for industrial wastewater treatment.

A high photocatalytic degradation efficiency of approximately 92% was achieved using 0.03 g of the NiO@WO₃-chitosan catalyst, and the degradation efficiency exhibited only a marginal decline to 91% after six consecutive reuse cycles, demonstrating excellent reusability and stability of the material [23]. A comparative summary of previously reported photocatalytic composites used for the degradation of TOOO, EBT, and other structurally similar dyes, along with their removal efficiencies, is presented in Table 2 to contextualize the novelty of the present work.

Despite numerous studies on the degradation of organic pollutants such as pesticides and synthetic dyes using metal oxide-based nanocomposites, limited research has specifically addressed the simultaneous removal of Tropaeolin OOO and Eriochrome Black T azo dyes **Figure 1,Table 1.**Furthermore, no studies to date have reported the application of a NiO@WO₃-chitosan nanocomposite synthesized via a green route for degrading these dyes under varied experimental conditions, including dye concentration, pH, and catalyst dosage.

The present study employs an eco-friendly, sustainable, and cost-effective green synthesis method to fabricate NiO@WO₃-chitosan nanocomposites using *Azadirachta indica* leaf extract. The phytochemicals present in the extract—such as quercetin, β-sitosterol, and polyphenolic flavonoids—act as natural surfactants and capping agents, facilitating the reduction and stabilization of metal oxide nanoparticles during synthesis [26]. This approach not only aligns with green chemistry principles but also avoids the use of hazardous reducing agents typically involved in conventional synthesis techniques.

While NiO@WO₃ composites have predominantly been synthesized using hydrothermal or electrochemical methods [24,25], the current green synthesis approach presents a more sustainable and scalable alternative suitable for industrial applications. The integration of NiO into WO₃ enables the formation of a p–n heterojunction, which narrows the effective band gap and enhances charge carrier separation, thereby improving photocatalytic performance under direct sunlight. However, the individual application of NiO and WO₃ is limited by their relatively large band gaps and rapid recombination of photogenerated electron–hole pairs, which restricts their overall efficiency [5,9,27].

By embedding the bimetallic oxide system within a chitosan matrix, the composite exhibits improved photocatalytic performance due to enhanced surface area, charge mobility, and pollutant adsorption capacity. This NiO@WO₃-chitosan nanocomposite demonstrated high photocatalytic efficiency, structural stability, and excellent reusability—maintaining activity through at least eight successive degradation cycles—thereby underlining its potential for practical environmental remediation.

The present investigation not only establishes the effective photodegradation of TOOO and EBT azo dyes under sunlight but also provides insights into the reaction kinetics and degradation pathways. Additionally, the nanocomposite's morphology, crystallinity, and surface characteristics were systematically characterized. This study contributes a novel and sustainable strategy for addressing emerging organic pollutants and provides a valuable foundation for the future development of green photocatalytic systems.

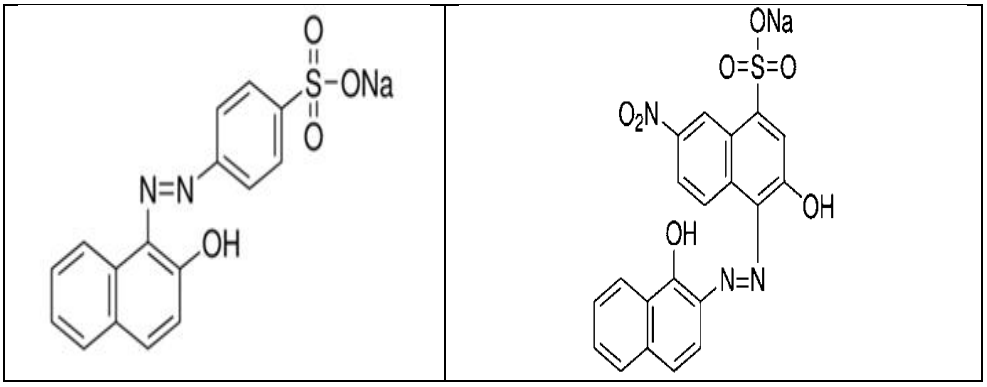

Figure 1. Chemical property of Tropaeolin OOO and Eriochrome blackT EBT.

Table 1. Chemical properties of Tropaeolin OOO (TOOO) and Eriochrome Black T (EBT)

Property	Tropaeolin OOO (TOOO)	Eriochrome Black T (EBT)
Chemical formula	$C_{16}H_{13}N_2NaO_5S$	$C_{20}H_{12}N_3NaO_7S$
Molecular weight (g/mol)	368.34	461.43
Functional groups	–SO_3Na, –N=N–, –OH	–SO_3Na, –N=N–, –OH, –COOH
(nm)	~430 nm	~530 nm
Appearance	Orange-red powder	Dark violet to black powder
Solubility	Soluble in water	Soluble in water
Application	pH indicator, dye in textile/lab applications	Complexometric indicator, textile dye, pH indicator

Table 2. Comparison of photocatalytic degradation of Tropaeolin OOO (TOOO) and Eriochrome Black T (EBT) using different nanocomposites under various conditions.

Photocatalyst	Target Dye	Catalyst Dose (g/L)	Light Source	Degradation (%)	Time (min)	Reference
ZnO-Ag	TOOO	0.05	UV	84	120	[18]
ZnO@WO_3	TOOO	0.03	Sunlight	88	90	[—]
NiO@ZnO	EBT	0.04	Visible light	85	120	[—]
SnO_2-rGO	EBT	0.02	UV	90	60	[—]
$CuMn_2O_4$/Chitosan	Methylene Blue	0.01	Sunlight	99	60	[15]
$CuMn_2O_4/Mn_2O_3$	Remazol Brilliant Blue R (RBBR)	0.03	Sunlight	78.12	90	[22]
NiO@WO_3-Chitosan (Present study)	TOOO, EBT	0.03	Sunlight	96 (TOOO), 92 (EBT)	180	This work

II. EXPERIMENTAL

2.1 Reagents and Materials

Sodium tungstate dihydrate (96% extra pure), nickel chloride (97%), hydrochloric acid (35% extra pure), sodium hydroxide (≥90%), chitosan (with 75% degree of deacetylation), Eriochrome Black T, and Tropaeolin OOO (extra pure) were procured from LOBA Chemie, India. All experiments were conducted using deionized water as the solvent. Fresh leaves of *Azadirachta indica* were collected from the institute campus. Approximately 20 g of leaves were thoroughly washed three times with deionized water to remove surface impurities, then finely ground and centrifuged to obtain a clear aqueous extract, which was subsequently stored at 5 °C until further use.

2.2 Green Synthesis of NiO, WO_3, NiO@WO_3, and NiO@WO_3-Chitosan Nanocomposite

The NiO@WO_3-chitosan nanocomposite was synthesized by mixing equimolar (0.1 M, 100 mL) aqueous solutions of nickel chloride and sodium tungstate with 2 mL of *Azadirachta indica* leaf extract under continuous stirring at 50 °C for 1 hour. Subsequently, chitosan solution (20% w/v in 50 mL acetic acid) and sodium hydroxide solution (0.1 M) were added dropwise simultaneously over a period of 1 hour to the reaction mixture. The resulting precipitate was collected by filtration, dried in an oven at 80 °C, and then calcined in a muffle furnace at 200 °C for 4 hours. A schematic illustration of the nanocomposite synthesis procedure is presented in Figure 2. For comparative analysis, individual NiO, WO_3, and NiO@WO_3 samples were synthesized using similar protocols.

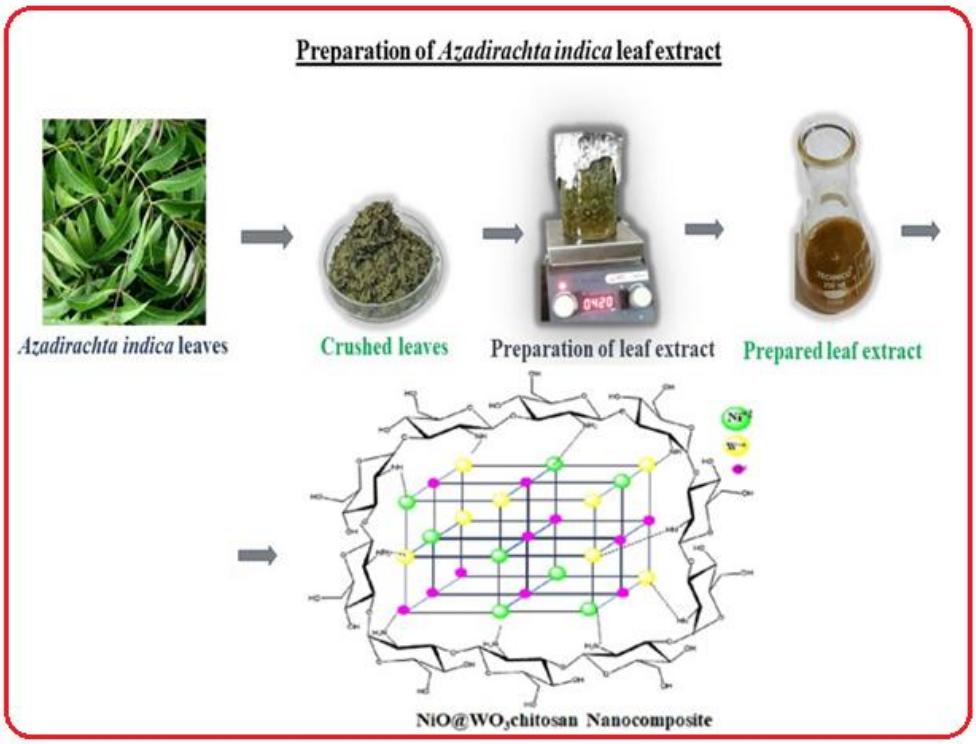

Figure 2. Schematic illustration of the synthesis procedure of the NiO@WO_3–chitosan nanocomposite using *A. indica*.

III. RESULTS AND DISCUSSION

3.1. PXRD Analysis

The crystalline and amorphous nature, lattice strain, crystallite size, and crystal structure of the nanocomposite were investigated using powder X-ray diffraction (PXRD). In the PXRD pattern of WO_3, the peak with the highest intensity was observed at $2\theta = 23.1°$, corresponding to a d-spacing of 0.38 nm and Miller indices (100), with additional peaks . The WO_3 exhibited a monoclinic crystal structure with lattice parameters a = 0.38 nm, b = c = 0.75 nm, and angles $\alpha = \beta = \gamma = 90°$. These data are in good agreement with the ICSD reference card No. 98-001-5905 [32]. For the NiO composite, the most intense peak appeared at $2\theta = 33.06°$, with a d-spacing of 0.271 nm and Miller index (001). These values align well with ICSD card No. 98-064-6096 [35]. The lattice parameters for NiO were determined as a = b = 0.298 nm, c = 0.516 nm, with angles $\alpha = \beta = 90°$ and $\gamma = 120°$, consistent with a face-centered cubic crystal system [33],

The PXRD pattern of the NiO@WO_3-chitosan nanocomposite displayed a maximum intensity peak at $2\theta = 43.19°$ with a d-spacing of 0.2095 nm and Miller index (011). Additional peaks were observed at 31.66°, 37.25°, 45.45°, 46.67°, 51.81°, 62.83°, 68.21°, and 75.36°, corresponding to Miller indices (001), (010), (080), (098), (011), (198), (020), (002), and (120), respectively, confirming the sample's phase purity. The composite exhibited a tetragonal crystal structure with lattice parameters a = b = 1.5406 Å, c = 1.39 Å, and angles $\alpha = \beta = \gamma = 90°$. Broadened peaks observed in the NiO@WO_3-chitosan composite are attributed to the polymeric chitosan coating, while sharp peaks confirm the crystalline framework. Overall, the nanocomposite demonstrates semi-crystalline behavior. The chitosan polymer coating did not induce additional peaks in the PXRD pattern, indicating that it does not alter the crystal planes of the nanocomposite Figure 3 [13].

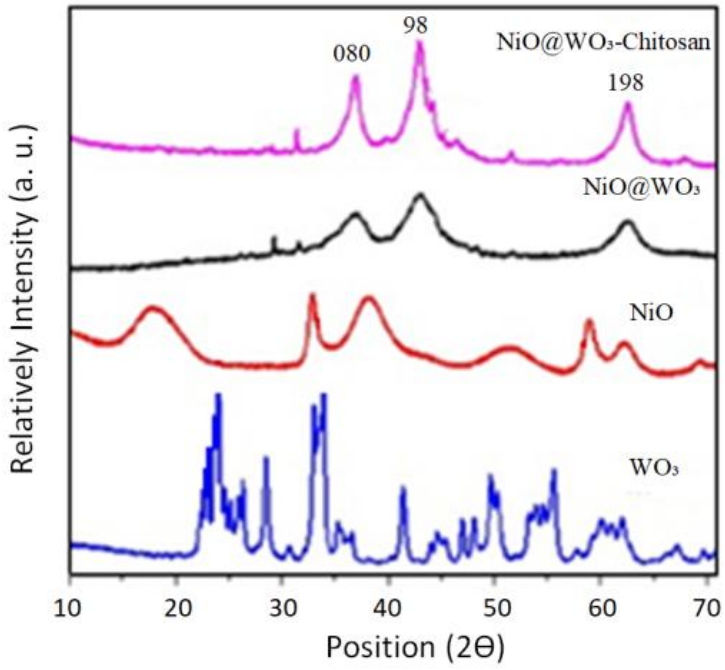

Figure 3. PXRD pattern of the NiO@WO_3–chitosan nanocomposite. The average crystallite size was calculated using Scherrer's equation:

$D = \lambda K/\beta\cos\theta$

where λ\lambdaλ represents the X-ray wavelength, θ\thetaθ is the Bragg diffraction angle, β\betaβ denotes the full width at half maximum (FWHM) of the diffraction peak in radians, and KKK is the shape factor, typically valued at 0.99 [48]. The crystallite sizes determined for the samples were 14.3 nm for NiO@WO_3-chitosan, 40.0 nm for NiO@WO_3, 77.2 nm for NiO, and 45.5 nm for WO_3.

The lattice strain (ε\varepsilonε) was calculated using the relation:

−1(1)LatticeStrainC=βhkl4tanθ
Additionally, the dislocation density (δ\deltaδ) was estimated by:
δ=1D2
where Dis the crystallite size [37].

The observed decrease in both dislocation density and lattice strain indicates effective incorporation of NiO and WO_3 within the chitosan polymer matrix, resulting in improved structural integrity of the nanocomposite.

3.2. Surface Morphology Analysis by FE-SEM

The surface morphology, particle size, and elemental composition of the nanocomposite were investigated using gold-coated field emission scanning electron microscopy (FE-SEM) [38]. The NiO sample exhibited small spherical particles, while WO_3 displayed rod-like clustered structures. The NiO@WO_3-chitosan composite demonstrated predominantly spherical morphology with an average particle size of approximately 100 nm (Fig. 4a).

Energy dispersive spectroscopy (EDS) analysis revealed the elemental composition of the NiO@WO_3-chitosan nanocomposite as O (50.01%), C (27.74%), Ni (12.45%), and W (9.79%) (Fig. 4b). These results confirm the successful encapsulation of metal oxides by the chitosan polymer matrix. The relatively high percentages of carbon and oxygen elements are attributed to phytochemicals present in the plant extract as well as the chitosan polymer. The presence of these phytochemicals on the nanocomposite surface plays a critical role in the degradation mechanism and contributes to the enhanced stability of the NiO@WO_3-chitosan nanocomposite.

Particle size distribution analysis, conducted using ImageJ software, showed size ranges of 60–80 nm for NiO@WO_3-chitosan, 80–100 nm for NiO@WO_3, 80–120 nm for NiO, and 60–80 nm for WO_3, consistent with FE-SEM observations (Fig. 4c). Variations in morphology are attributed to differences in polarity, molecular structure, and polymer presence, which significantly influence crystal growth, aggregation, and nucleation processes [39].

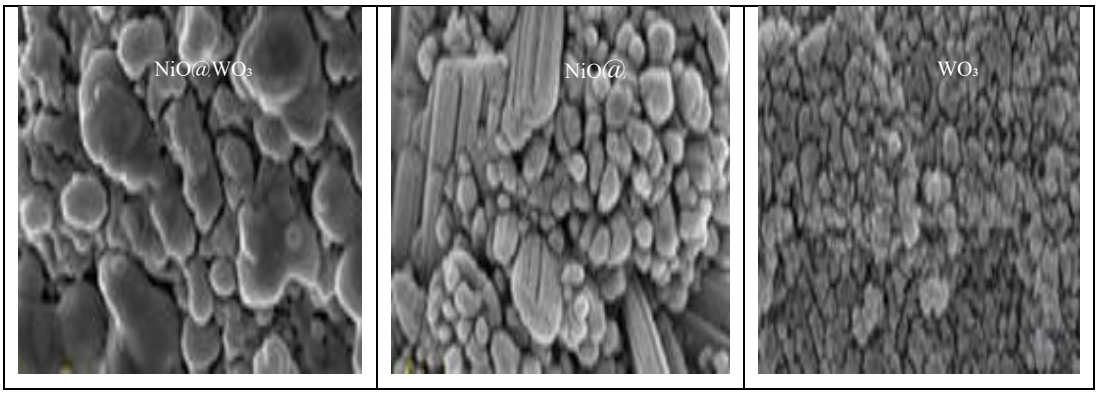

Figure 4. FE-SEM images illustrating the morphological features of NiO@WO_3–chitosan, NiO@WO_3, WO_3, and NiO nanocomposites, indicating the effect of chitosan and bimetallic composition on surface structure.

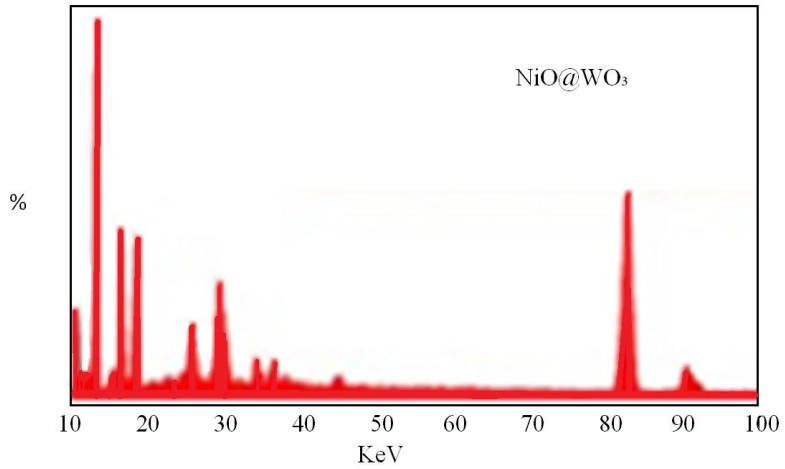

Figure 5..Energy-dispersive X-ray (EDX) spectra of the NiO@WO_3–chitosan nanocomposite, confirming the presence of Ni, W, O, and C elements and verifying the successful formation of the nanocomposite.

3.3. Band Gap Calculation by UV–Vis Spectroscopy

The band gaps of the synthesized nanocomposites NiO@WO_3-chitosan, NiO@WO_3, NiO, and WO_3 were determined using UV–Vis absorption spectroscopy within the wavelength range of 200–800 nm. The electronic transitions between the valence and conduction bands were analyzed following the Tauc method, where the band gap energy is derived from the absorption coefficient (α), as detailed in the supplementary information [41]. The measured band gap values for NiO@WO_3-chitosan, NiO@WO_3, NiO, and WO_3 were found to be 2.1 eV, 2.4 eV, 3.4 eV, and 2.6 eV, respectively (Fig. 6). The observed band gap shift in the composite confirms successful doping during synthesis, which correlates with enhanced photocatalytic activity. Notably, the incorporation of chitosan reduced the band gap of NiO@WO_3 from 2.4 eV to 2.1 eV. Similar band gap modifications have been reported in other doped composites such as ZnO@UF (1.3 eV), ZnS@UF (1.8 eV), N-Bi_2O_3@SnO_2, and ZnO@CdS (1.67 eV) following doping treatments [26, 47].

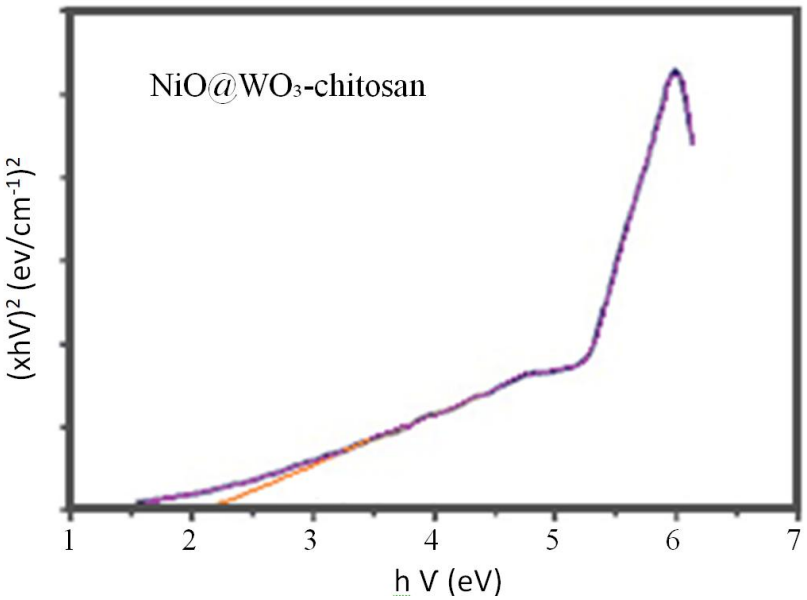

Figure.6. Band gap analysis of synthesized nanocomposites NiO@WO_3-chitosan, NiO@WO_3, WO_3, and NiO determined by UV–Vis absorption spectroscopy.

3.4. Photocatalytic Degradation of TOOO and EBT Dye

The photocatalytic degradation of Tropaeolin OOO (TOOO) and Eriochrome Black T (EBT) dyes using the NiO@WO_3-chitosan nanocomposite was investigated under various reaction parameters, including pollutant concentration (10 to 50 mg L^{-1}), catalyst dosage (5 to 25 mg), and pH range (3 to 11). Comparative experiments were also conducted using parent nanoparticles (NiO@WO_3, NiO, and WO_3), as shown in Figure.7.

Under natural sunlight irradiation for 3 hours, at neutral pH and with a catalyst dosage of 20 mg for 10 mg L^{-1} pollutant concentration, the maximum degradation efficiencies were approximately 96% for TOOO and 92% for EBT. An increase in dye concentration led to a decline in degradation efficiency, attributed to the limited availability of active sites on the catalyst surface and a reduced generation of hydroxyl radicals, thereby decreasing the degradation rate [13], [22].

Catalyst dosage studies revealed that increasing the amount of NiO@WO_3-chitosan up to 20 mg enhanced degradation; however, beyond this dose, the degradation rate plateaued (Fig. 7). This phenomenon is likely due to increased solution turbidity at higher catalyst concentrations, which hinders light penetration and reduces the effective volume for photon absorption, consequently lowering the degradation efficiency [40]. Additionally, excessive catalyst dosages can lead to greater molecular collisions, producing inactive radical species and further diminishing photocatalytic performance [31], [20].

The pH of the reaction medium critically influences photocatalytic activity. Optimal degradation of TOOO and EBT dyes at 10 mg L^{-1} was observed near neutral pH (7) with 20 mg catalyst dosage (Fig. 7). This behavior is related to the surface charge characteristics of the nanocomposite and the ionic nature of the dyes. Metal oxides with point of zero charge (PZC) values around 6.5 typically exhibit enhanced photocatalytic activity near neutral pH [13]. The synthesized NiO and WO_3 nanoparticles possess basic PZC values (>7.0). Both TOOO and EBT dyes contain sulfonic groups, conferring anionic properties(50). These negatively charged dye molecules interact favorably with the positively charged catalyst surface at pH values below the PZC, facilitating adsorption and subsequent degradation.

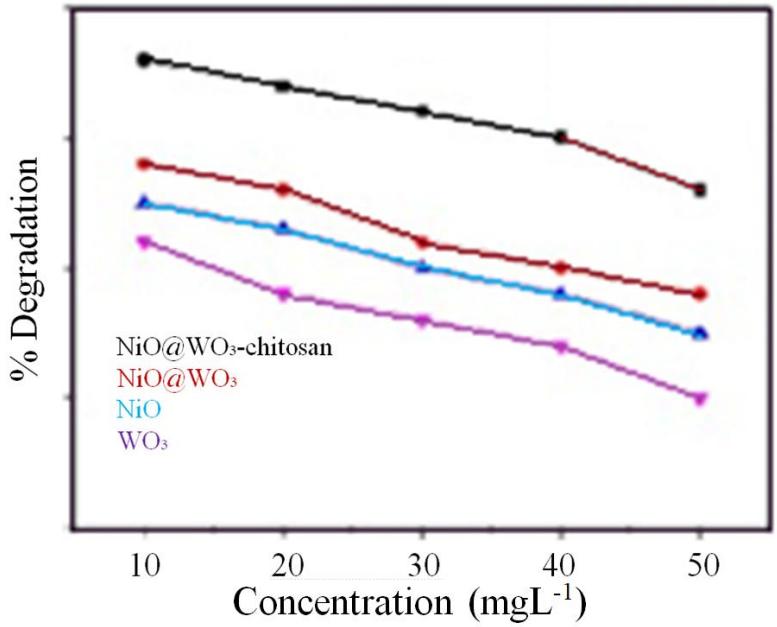

Figure 7. Photocatalytic degradation study of TOOO dye using NiO@WO₃, WO₃, and NiO as catalysts. The effects of dye concentration, catalyst dosage, and pH on the degradation efficiency are presented.

3.6.1 Proposed Chemical Kinetics for TOOO and EBT Removal

The kinetics of photocatalytic degradation of the organic dyes TOOO and EBT were evaluated under optimal conditions: maximum contaminant concentration, neutral pH, and a catalyst dosage of 20 mg. Both dyes exhibited a decrease in concentration consistent with first-order reaction kinetics. The NiO@WO₃-chitosan nanocomposite demonstrated enhanced photocatalytic activity over time, attributed to the generation of electrons on the catalyst surface under sunlight exposure. These electrons facilitate the formation of hydroxyl and superoxide radicals, which effectively oxidize the organic dyes TOOO and EBT, leading to rapid degradation [30], [33]. The maximum degradation efficiencies reached 96% for TOOO and 92% for EBT after 3 hours of sunlight irradiation.

The degradation of TOOO and EBT dyes is primarily governed by π-π interactions with the photocatalyst surface. Kinetic parameters including the rate constant (k), half-life ($t_{1/2}$), coefficient of determination (R^2), and p-values for the nanocomposite are summarized in Table 3. The NiO@WO₃-chitosan composite exhibited a low half-life and a high rate constant, indicating superior degradation efficiency compared to other materials.

Adsorption isotherm analysis further supported the degradation mechanism, with the Langmuir isotherm model best fitting the experimental data for both dyes, as evidenced by the highest R^2 values (Fig. 8) compared to other models. The Langmuir model also demonstrated the lowest overall experimental error, validating its appropriateness for describing the adsorption process in this study [51-52]. This model implies homogeneous adsorption sites and monolayer coverage of dye molecules on the catalyst surface [19], [45].

The maximum sorption capacity (X_m), affinity constant (K_L), and correlation coefficient (R^2) for TOOO and EBT dyes followed the trend: NiO@WO₃-chitosan (14.51 mg/g, 0.94, 0.925) > NiO@WO₃ (11.15 mg/g, 0.95, 1.83) > NiO (7.42 mg/g, 0.93, 2.66) > WO₃ (8.22 mg/g, 0.93, 2.89) for TOOO, and NiO@WO₃-chitosan (20.73 mg/g, 0.97, 0.21) > NiO@WO₃ (18.54 mg/g, 0.99, 0.75) > NiO (6.16 mg/g, 0.97, 6.8) > WO₃ (9.22 mg/g, 0.98, 2.9) for EBT, respectively. Additional kinetic parameters and model fits are provided Overall, the NiO@WO₃-chitosan nanocomposite exhibited superior photocatalytic degradation performance for both TOOO and EBT dyes compared to their respective pristine nanoparticles.

Table 3. Kinetic parameters including the rate constant (k, h^{-1}), half-life ($t_{1/2}$, h), and correlation coefficient (R^2) for the photocatalytic degradation of TOOO and EBT dyes under optimized conditions.

Catalyst	TOOO *k* (h^{-1})	TOOO $t_{1/2}$ (h)	TOOO R^2	EBT *k* (h^{-1})	EBT $t_{1/2}$ (h)	EBT R^2
NiO@WO₃-Chitosan	0.26	2.68	0.980	0.19	3.64	0.978
NiO@WO₃	0.21	3.30	0.990	0.13	5.33	0.980
NiO	0.19	3.64	0.980	0.10	6.93	0.980
WO₃	0.15	4.62	0.990	0.09	7.73	0.997

Catalyst	TOOO k (h^{-1})	TOOO $t_{1/2}$ (h)	TOOO R^2	EBT k (h^{-1})	EBT $t_{1/2}$ (h)	EBT R^2
Blank	0.01	69.30	0.990	0.02	34.65	0.998

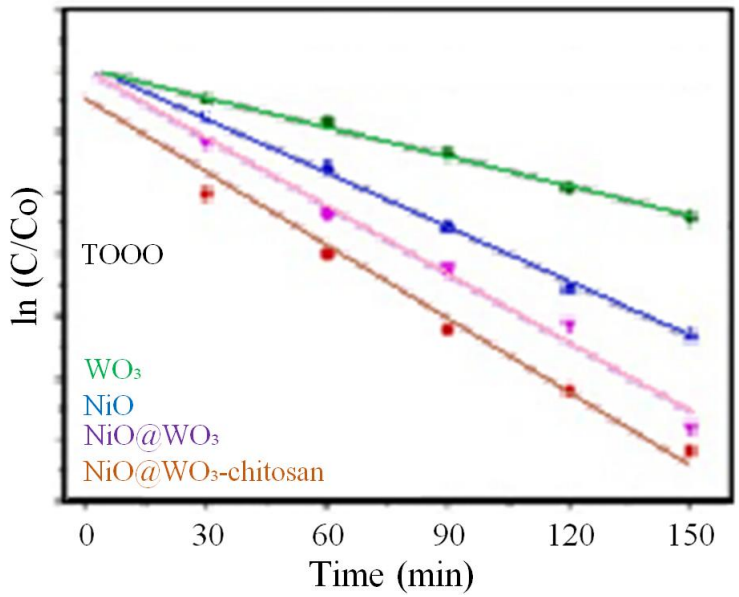

Figure 8. Kinetic analysis of TOOO and EBT dye degradation, along with Langmuir adsorption isotherm plots for both dyes under optimized conditions.

3.6.2. Degradation Pathway Analysis by LC-MS

Degradation pathways of TOOO and EBT dyes were determined by LC–MS analysis. The identified intermediates confirmed azo bond cleavage via hydroxyl radical (•OH) attack. For EBT, intermediates such as naphthalene-1-ol (m/z = 141) and 2-nitronaphthalene (m/z = 73) indicated •OH-induced breakdown of the azo linkage. TOOO degradation yielded naphthalene-1-ol (m/z = 144) and hexa-1,3,5-trien-1-ol (m/z = 98), which further transformed into simpler, non-toxic products under continued •OH attack.

3.7. Reusability of NiO@WO₃–Chitosan for Dye Degradation

The NiO@WO₃–Chitosan composite was tested for the degradation of TOOO and EBT dyes under solar irradiation using a 20 mg catalyst dose. The composite exhibited higher degradation efficiency compared to its individual components (NiO@WO₃, NiO, and WO₃).

To evaluate the reusability of the catalyst, repeated degradation experiments were performed over eight consecutive cycles. After each cycle, the catalyst was recovered by filtration and washed with deionized water and acetone. Even after the eighth reuse, the NiO@WO₃–Chitosan composite maintained more than 80% of its initial degradation efficiency. The slight decrease in performance was attributed to minor catalyst loss during the recovery and washing steps.

PXRD analysis was carried out after the first and eighth cycles to examine the structural stability of the composite. Only minor changes were observed, confirming the robustness and durability of the NiO@WO₃–Chitosan material during repeated use (Fig. 9).

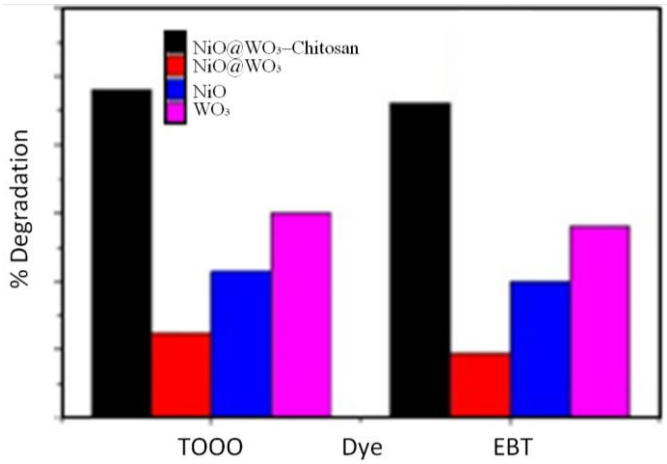

Figure 9. Bar chart showing the percentage degradation of TOOO and EBT dyes under sunlight irradiation in the presence of different radical scavengers.

IV. CONCLUSIONS

The NiO@WO_3–chitosan nanocomposite was successfully synthesized through an environmentally friendly and cost-effective green route using *Azadirachta indica* plant extract as both a reducing and stabilizing agent. Spectroscopic and microscopic characterizations confirmed the formation of clean, semi-crystalline, and uniformly distributed spherical nanoparticles with average sizes ranging from 15 to 30 nm. The distinct and broad diffraction peaks observed in the PXRD pattern further verified the semi-crystalline nature and phase purity of the synthesized composite.

The NiO@WO_3–chitosan composite exhibited remarkable photocatalytic activity toward the degradation of organic dyes, achieving degradation efficiencies of 96% for TOOO and 92% for EBT within 150 minutes under solar irradiation. The photodegradation process followed pseudo-first-order kinetics and fitted well with the Langmuir adsorption isotherm, indicating monolayer adsorption of dye molecules on the catalyst surface. The enhanced photocatalytic performance can be attributed to several synergistic factors, including the reduced band gap energy (2.1 eV), high surface area, small particle size, and highly negative zeta potential (−29.5 mV), which collectively improve light absorption, charge separation, and dye adsorption.

Furthermore, the composite demonstrated excellent reusability and structural stability, retaining over 80% of its photocatalytic efficiency even after eight consecutive cycles. PXRD analysis after repeated use confirmed the preservation of the crystalline structure, highlighting the robustness of the material under prolonged irradiation and recycling conditions.

In conclusion, the green-synthesized NiO@WO_3–chitosan nanocomposite represents a promising, sustainable, and reusable photocatalyst for the efficient removal of organic pollutants from wastewater. Its eco-friendly synthesis, superior photocatalytic activity, and long-term stability underscore its potential for large-scale applications in environmental remediation and water purification technologies.

REFERENCES

[1]. S. Parmar, S. Daki, S. Bhattacharya, A. Shrivastav.Microorganism: An ecofriendly tool for waste management and environmental safety, Development in Wastewater Treatment Research and Processes, Elsevier (2022), pp. 175-193
[2]. V. Chandanshive, S. Kadam, N. Rane, B.H. Jeon, J. Jadhav, S. Govindwar.,In situ textile wastewater treatment in high-rate transpiration system furrows planted with aquatic macrophytes and floating phytobeds.Chemosphere, 252 (2020), p. 126513
[3]. G. Shukla, M. RaniU.Shanker, Sustainable nanohybrid of CaO with rGO for efficient photocatalytic removal of wastewater pollutantsEnviron.Nanotechnol. Monit. Manage., 20 (2023), Article 100889
[4]. S.S. Hemdan, Al Jebaly, F.K. AliThe behaviour and properties of some acid-base indicators: a reviewJ Sci Hum Stu, 66 (2020), pp. 1-22
[5]. A.M. Elgarahy, K.Z. Elwakeel, S.H. Mohammad, G.A. ElshoubakyA critical review of biosorption of dyes, heavy metals and metalloids from wastewater as an efficient and green processCleaner Eng. Technol., 4 (23) (2021), pp. 567-575
[6]. R. Kishor, D. Purchase, G.D. Saratale, R.G. Saratale, L.F.R. Ferreira, M. Bilal, R.N. Bharagava.Ecotoxicological and health concerns of persistent coloring pollutants of textile industry wastewater and treatment approaches for environmental safety
[7]. J. Environ. Chem. Eng., 9 (2) (2021), p. 105012
[8]. P. Manickam, D. VijayChemical hazards in textiles, Chemical Management in Textiles and Fashion, Woodhead Publishing (2021), pp. 19-52, 10.1016/B978-0-12-820494-8.00002-2
[9]. Y. Feng, X. Wang,Antioxidant therapies for Alzheimer's diseaseOxid. Med. Cell. Longev., 7 (2012), pp. 687-1616
[10]. G.Duoerkun Zhang Y., Z. Shi, X. Shen, W. Cao, T. Liu, J. Liu, Q. Chen, L. Zhang Construction of n-TiO_2/p-Ag_2O junction on carbon fiber cloth with Vis–NIR photoresponse as a filter-membrane-shaped photocatalyst.Adv. Fiber Mater., 2 (2020), pp. 13-23
[11]. [M. Rachna, U. Rani.Shanker, Synergistic effects of zinc oxide coupled copper hexacyanoferrate nanocomposite: robust visible-light driven dye degradation J. Colloid Interface Sci., 584 (2021), pp. 67-79

[12]. M. Keshu Shanker, U. Rani.Highly efficient removal of endocrine disrupting pesticides by metal ferrites loaded Guar gum based green nanomaterialsJ. Mol. Liq., 387 (2023), Article 122611

[13]. H. Yin, F. Yao, Z. Pi, Y. Zhong, L. He, K. Hou, Q. YangEfficient degradation of bisphenol A via peroxydisulfate activation using in-situ N-doped carbon nanoparticles: structure-function relationship and reaction mechanis.J. Colloid Interface Sci., 586 (2021), pp. 551-562

[14]. X. Zhang, T. Bhattacharya, C. Wang, A. Kumar, P.V. Nidheesh.Straw-derived biochar for the removal of antibiotics from water: Adsorption and degradation mechanisms, recent advancements and challenges.Environ. Res. (2023), p. 116998

[15]. M. Rani, U. Shanker Keshu.Sunlight-induced photocatalytic degradation of organic pollutants by biosynthesized heterometallic oxides nanoparticlesEnviron Sci. Pollut. Res., 28 (43) (2021), pp. 61760-61780, 10.1007/s11356- 021-15003-0

[16]. M.S. Kazemi, A. SobhaniCuMn2O4/chitosan micro/nanocomposite: Green synthesis, methylene blue removal, and study of kinetic adsorption, adsorption isotherm experiments, mechanism and adsorbent capacity,Arab. J. Chem., 16 (6) (2023), p. 104754

[17]. A. Hayat, S.K.B. Mane, N. Shaishta, J. Khan, A. Hayat, G. Keyum, G. Manjunatha Nickel oxide nano-particles on 3D nickel foam substrate as a non-enzymatic glucose sensor J. Electrochem. Soc., 166 (15) (2019), p. B1602

[18]. S. Yao, X. Zhang, F. Qu, A. Umar, X. Wu.Hierarchical WO3 nanostructures assembled by nanosheets and their applications in wastewater purificationJ Alloy. Compd., 689 (2016), pp. 570-574

[19]. S.J. Bailon-Ruiz, Y. Cedeño-Mattei, K. Torres-Torres, L. Alamo-Nole Photodegradation of tropaeolin O in the presence of Ag-doped ZnO nanoparticles Micro, 3 (2023), pp. 643-652

[20]. M. Rani, U. Keshu.Shanker, Sunlight-induced photocatalytic degradation of organic pollutants by biosynthesized heterometallic oxides nanoparticles Environ. Sci. Pollut. Res., 2843 (2021), pp. 61760-61780, 10.1007/s11356- 021-15003-0

[21]. M. Rani, U. Shanker.Efficient removal of plastic additives by sunlight active titanium dioxide decorated Cd–Mg ferrite nanocomposite: green synthesis, kinetics and photoactivity.Chemosphere, 290 (2022), p. 133307

[22]. Alinavaz.Co-precipitation synthesis of $CuMn_2O_4$/CuMnO nanocomposites without capping agent and investigation of their applications for removing pollutants from wastewaterBiomass Convers,Biorefin., 111 (2023)

[23]. A. Sobhani.$CuMn_2O_4$/Mn_2O_3 micro composites: Sol-gel synthesis in the presence of sucrose and investigation of their photocatalytic propertiesArab. J. Chem., 16 (10) (2023), p. 105201

[24]. A. Sobhani, S. Alinavaz.ZnMn2O4 nanostructures: Synthesis via two different chemical methods, characterization, and photocatalytic applications for the degradation of new dyes,Heliyon, 9 (11) (2023)

[25]. D. Rani.Rosaline, S.S.R. Inbanathan, A. Suganthi, M. Rajarajan, G. Kavitha, R. Srinivasan, E. Manikandan,Visible-light driven photocatalytic degradation of eosin yellow (EY) dye based on NiO-WO3 nanoparticles.J. Nanosci. Nanotechnol., 20 (2) (2020), pp. 924-933

[26]. M. Rani, U. Shanker.Sunlight-assisted degradation of toxic phenols by zinc oxide doped Prussian blue nanocomposite.Int. J. Environ. Sci. Technol., 8 (4) (2020), p. 104040

[27]. Q. Yang.Efficient degradation of bisphenol A via peroxydisulfate activation using in-situ N-doped carbon nanoparticles: structure-function relationship and reaction mechanismJ.Colloid Interface Sci., 586 (2021), pp. 551-562

[28]. S. Yao, X. Zhang, F. Qu, A. Umar, X. Wu.Hierarchical WO3 nanostructures assembled by nanosheets and their applications in wastewater purification.J. Alloy. Compd., 689 (2016), pp. 570-574

[29]. S.J. Bailon-Ruiz, Y. Cedeño-Mattei, K. Torres-Torres, L. Alamo-Nole.Photodegradation of tropaeolin O in the presence of Ag-doped ZnO nanoparticles.Micro, 3 (2023), pp. 643-652

[30]. K. Torres-Torres, V.I. Nash-Montes, J. Luciano-Velázquez, S.J. Bailón-Ruiz Degradation of amaranth and tropaeolin O in the presence of ZnO nanoparticles.Int. Nano Lett., 12 (3) (2022), pp. 295-300

[31]. R.B. Mampilly, S.H. Bhatt, N.J. Modi, A. Pathan.Adsorption of Eriochrome Black-T dye by batch investigations using waste tea@ Fe NPs as low-cost adsorbent. Int. J. Thin Film. Sci. Technol., 13 (1) (2024), pp. 17-25

[32]. A. Sajid, R. Javed, Q. Manzoor, A. Sajid, A. Saleem, F. Imtiaz, H. Nadeem.,Development of Ag–CeO2 bimetallic nanocomposite for visible-light-induced photocatalytic degradation of eriochrome black T.Chem. Africa (2024), pp. 1-8

[33]. H. Hajjaoui, A. Soufi, H. Khiar, M. Abdennouri, M. Achak, N. Barka.Preparation of sodium zinc phosphate/polyaniline nanocomposite for Cr (VI) and eriochrome black T adsorption from water.Mater. Today Commun., 36 (2023), p. 106755

[34]. V. Kumari, S. Kaushal, P.P. Singh.Green synthesis of a CuO/rGO nanocomposite using a Terminalia arjuna bark extract and its catalytic activity for the purification of water Materials Adv, 3 (4) (2022), pp. 2170-218

[35]. T.L. Kwong, K.F. Yung.Surfactant-free microwave-assisted synthesis of Fe-doped ZnO nanostars as photocatalyst for degradation of tropaeolin O in water under visible light.J.Nanomater., 16 (1) (2015),p. 199 J. Yadav, M. Rani, T.C. Zhang, U. Shanker.Efficient photo-adsorptive eradication of endocrine disrupting pesticides by chitosan co-decorated metal oxide bio-nanocomposite.Environmental Science and Pollution Research, 30 (28) (2023), pp. 72523-72538

[36]. N.P. Raval, G.V. Priyadarshi, S. Mukherjee, H. Zala, D. Fatma, A. Bonilla-Petriciolet, M.H. Trivedi.Statistical physics modeling and evaluation of adsorption properties of chitosan-zinc oxide nanocomposites for the removal of an anionic dye J. Environ. Chem. Eng., 10 (6) (2022), Article 108873

[37]. M. Rani, U. Shanker Keshu.Efficient visible light photocatalytic organic colorants elimination performance induced by biosynthesized titanium dioxide coupled cadmium sulfide nanostructures.Int. J. Environ. Sci. Technol., 20 (5) (2023), pp. 5491-5508

[38]. M.A. Ramu, M.S. Kumari, H.H. Elshikh, A.F. Alkhamis, D.C. Alrefaei.Chemosphere, 271 (2021), Article 129475

[39]. M. Keshu, U. Rani.Shanker, highly efficient removal of endocrine disrupting pesticides by metal ferrites loaded Guar gum based green nanomaterials,J. Mol. Liq., 387 (2023), Article 122611

[40]. A. Sajid, R. Javed, Q. Manzoor, A. Sajid, A. Saleem, F. Imtiaz, H. Nadeem Development of Ag–CeO2 bimetallic nanocomposite for visible-light-induced photocatalytic degradation of eriochrome black T.Chem. Africa (2024), pp. 1-8

[41]. M. Rani, S. Choudhary, G. Shukla, U. Shanker.Highly efficient photo-adsorptive degradation of tetracycline and metronidazole antibiotics by green synthesized Ag doped CeO2@ SnO2 nanocomposites.Environmental Nanotechnology, Monitoring & Management, 100935 (2024)

[42]. R.K. Singh, B. Ruj, A.K. Sadhukhan, P. Gupta.Thermal degradation of waste plastics under non-sweeping atmosphere: Part 1: effect of temperature, product optimization, and degradation mechanism.J. Environ. Manage., 239 (2019), pp. 395-406

[43]. A.MajumdarU. Ghosh, A. Pal.,2D-Bi4NbO8Cl nanosheet for efcient photocatalytic degradation of tetracycline in synthetic and real wastewater under visible-light: infuencing factors, mechanism and degradation pathway.J. Alloy Compounds, 900 (2022), p. 163400.

[44]. S.S. Hemdan, A.M. Al Jebaly, F.K. Ali.The behaviour and properties of some acid-base indicators: a review.J. Sci. and Human, 66 (2020), pp. 1-22

[45]. K. Torres-Torres, V.I. Nash-Montes, J. Luciano-Velázquez, S.J. Bailón-Ruiz Degradation of amaranth and tropaeolin O in the presence of ZnO nanoparticles Int. Nano Lett., 12 (3) (2022), pp. 295-300
[46]. S. Vigneshwaran, P. Sirajudheen, C. Nabeena, S. Meenakshi.,In situ fabrication of ternary TiO2 doped grafted chitosan/hydroxyapatite nanocomposite with improved catalytic performance for the removal of organic dyes: experimental and systemic studies.Coll Surf A: Physicochem Eng Aspect, 611 (2021), Article 125789
[47]. M. Rani, S. Sharma, U. Shanker Keshu.,Biowaste-derived nanocomposite of calcium oxide incorporated in nickel oxide for efficient removal of organic pollutants Biomass Conversion and Biorefinery (2024), pp. 1-16
[48]. M. Rani, U. Shanker.,Green construction of biochar@ NiFe2O4 nanocomposite for highly efficient photocatalytic remediation of pesticides from agriculture wastewater Chemosphere, 352 (2024), p. 141337
[49]. A. Sabir, H. Idrees, M. Shafq, R.U. Khan.,Porous Polymers for Membrane Applications, CRC Press (2022), pp. 161-173
[50]. R. Kishor, D. Purchase, G.D. Saratale, R.G. Saratale, L.F.R. Ferreira, M. Bilal, R.N. Bharagava.,Ecotoxicologicaland health concerns of persistent coloring pollutants of textile industry wastewater and treatment approaches for environmental safety.J. Environ. Chem. Eng., 9 (2) (2021), p. 105012
[51]. O.A. Stasyuk, A.A. Voityuk, M. Solà, A.J. Stasyuk.,γ-graphynes with extended polyyne chains for efficient photoinduced electron transfer in complexes with fullerenes Carbon, 215 (2023), Article 118460
[52]. M. Rani, U. Shanker, B.S. Kaith, M. Sillanpää.,Green fabrication of fluorescent N-doped carbon quantum dots from Aegle marmelos leaves for highly selective detection of Fe3+ metal ions.Inorganic Chemistry Communications, 159 (2024), p. 111878
[53]. J. Yadav, M. Rani, T.C. Zhang, U. Shanker.,Efficient photo-adsorptive eradication of endocrine disrupting pesticides by chitosan co-decorated metal oxide bio- nanocomposite Environmental Science and Pollution Research (2023) 30(28): 10.1007/s11356-023-27376-5